**STSM REPORT**

**STSM Application number:** COST-STSM-BM1205-36070
**STSM Grantee:** Xana Delpueyo Español
**STSM title:** Analysis of spectral, 3D and blood flow data for the skin cancer diagnosis
**Home Institution:** Centre for Sensors, Instruments and Systems Development (CD6), Universitat Politècnica de Catalunya (UPC), Terrassa (Spain)
**Host Institution:** Laboratorie d'analyse et d'architecture des systems (LAAS-CNRS), Toulouse (FR)
**STSM period:** 2nd January 2017 – 17th March 2017

**STSM purpose:**

This mission focuses on the analysis of data acquired with a multiphotonic platform including multispectral 3D imaging, and blood flow analysis based on Optical Feedback Interferometry (OFI) for in-vivo imaging of skin cancer lesions, which has been proposed for a diagnosis service in the context of the European project Diagnoptics. The goal is to improve the detection ratio and the evaluation of the prognosis of skin cancer at earlier stages, compared with the conventional approach used nowadays such as dermoscopy.

**Description of the work carried out during the STSM:**

Introduction

The aim of the European Project DIAGNOPTICS was to launch a hospital service to help in the detection and the prognosis evaluation of the skin cancer at earlier stages. Besides examining the skin lesions from patients with conventional dermoscopy, physicians were asked to use the new techniques to complete the diagnosis of the lesion with the multiphotonic platform including a confocal microscopy system (MAVIG VivaScope®), which helped to decide if the cytology of the suspicious lesions was needed; and also with three non-invasive novel optical systems: a multispectral system to obtain spectral information of the skin tissue at different wavelengths, a 3D system which giving topographic information of the skin and an optical feed-back interferometry system (OFI) providing information of the blood flow. For the comfort and functionality of the platform, the different systems included in it were assembled in a medical cart (Figure 1). The measurements were done in two hospitals: Hospital Provincial i Clínic de Barcelona (Barcelona, Spain) and Università degli studi di Modena e Reggio Emilia (Modena, Italy).

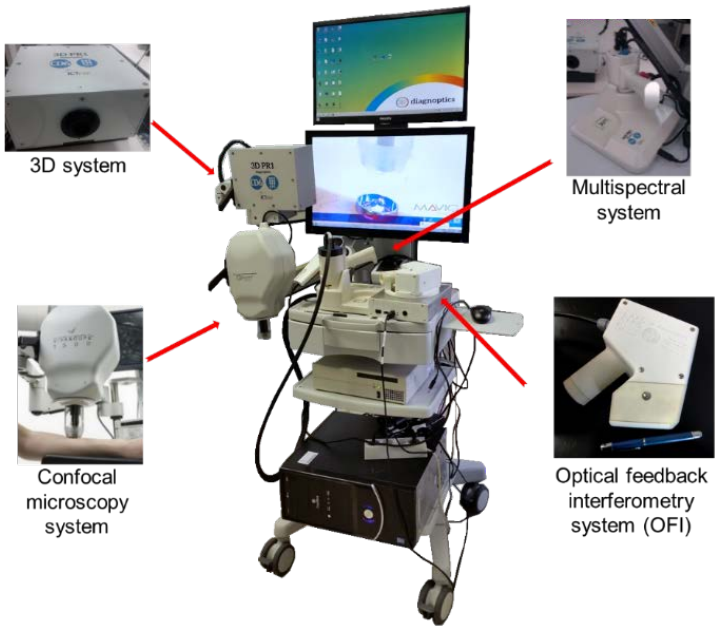


Figure 1. Medical cart with the confocal microscopy, the OFI, the 3D and the multispectral systems

The multispectral system has a cylindrical shape of about 10 cm in length and 7.5 of diameter attached to a conus of 4 cm length, with a height of 0.5 Kg. It includes a 12 bit-depth monochromatic camera and an objective lens, which allows recording skin lesions at 4 cm with a 15x20 mm field of view. A ring light source including 32 light-emitting diodes (LEDs) with 8 different peak wavelengths (414, 447, 477, 524, 671, 735, 890, 995 nm) illuminated the sample. This illumination source was located onward of the objective lens to avoid the light of the LEDs reaching the sensor directly. The spectral bands of the LEDs were chosen according to the spectral properties and absorption peaks of the skin chromophores and also taking into account the market availability of LEDs. Moreover, two polarizers allowed removing the specular reflection of the skin. Specifically, the first polarizer was located in front of the LEDs and the second in front of the objective lens. After the measurement of a lesion, 8 spectral images were obtained (Delpueyo et al. 2016).

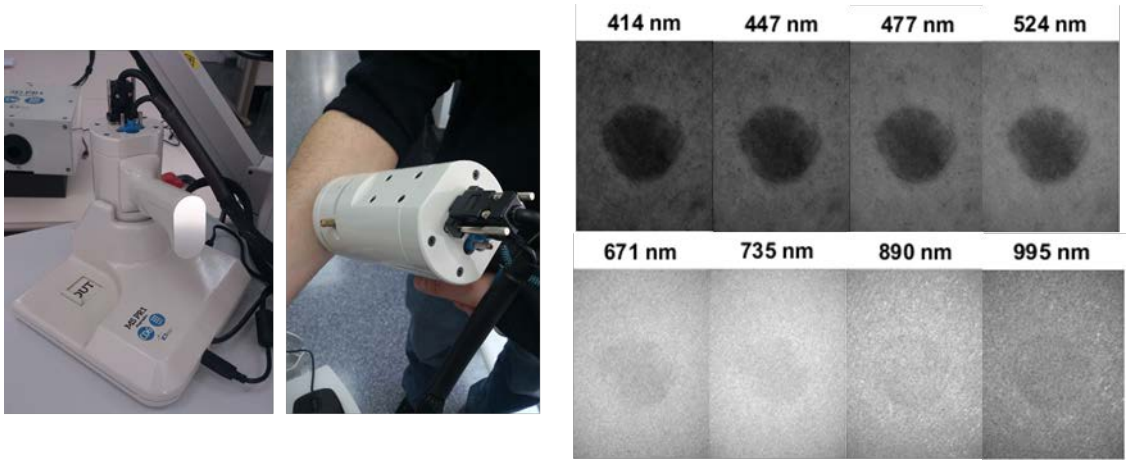


Figure 2. Multispectral system and reflectance image obtained from the spectral images.

The 3D system included in the platform used a stereoscopic optical technology which provides accurate 3D measurements of the human skin surface. It is worth noting that, nowadays, the palpation of the lesion is made in order to obtain information of lesion shape, border irregularity, and lesion diameter and so, 3D information is expected to bring more knowledge on skin cancer.

The system project fringes on the skin and is composed by two monochromatic cameras placed in a standard stereo geometry, a light picoprojector and a colour camera, placed both, in the middle of the cameras. All cameras had an objective lens with fixed focal length (25 mm) with a working distance of 110 mm, obtaining a field of view of 19x14 mm (Ares et al. 2014). The measuring principle was based on stereovision techniques combined with the projection of a sinusoidal pattern set shifted over the skin (Zhang 2010). For each projected pattern, both monochrome cameras captured the images in a synchronized way and after the measurement, the skin was uniformly illuminated with the projector in order to acquire a colour image of the lesion. Afterwards, the phase maps were unwrapped based on the Goldstein algorithm which allowed a good balance between a fast processing time and a good performance quality (Chen et al. 2005). Finally, the corresponding phases between both cameras were identified and the 3D data was obtained by triangulation based on the epipolar geometry (Laveau & Faugeras 1994) (Figure 3).

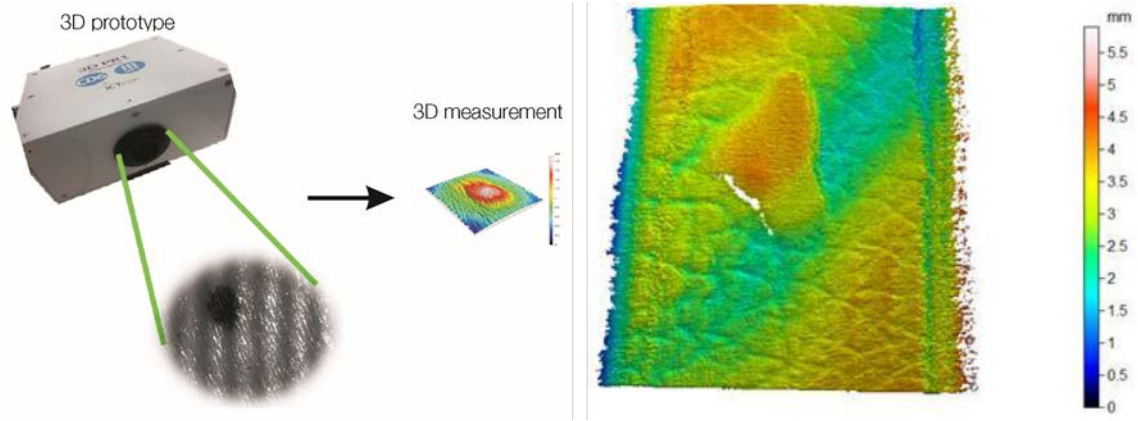


Figure 3. Fringes and topographic information obtained with the 3D system.

The OFI system used in this project consisted of a distributed feedback (DFB) laser diode emitting at 1310 nm, packaged with a monitoring photodiode located at the back facet of the laser which enabled the power variations acquisition induced by the interferences inside the active cavity of the laser, and a collimating lens placed in front of the laser to fit and keep the beam width along the optical path and onto the circular aluminium coated mirror of diameter 4.2 mm. A focusing lens was placed at its focal length form the target to focus the beam (Bosch et al. 2001; Moreira et al. 2016). Interferometric signal was recovered by monitoring of the laser output power or junction voltage. The system also included a base to provide the power supply, the signal acquisition card and the connections to the computer The system allowed to scan 225 different points in a 10x10 mm skin surface to obtain a 2D image of the lesion blood flow. The information provided at each measurement point by the OFI sensor is a parameter proportional to the blood perfusion level in the skin (Figure 4).

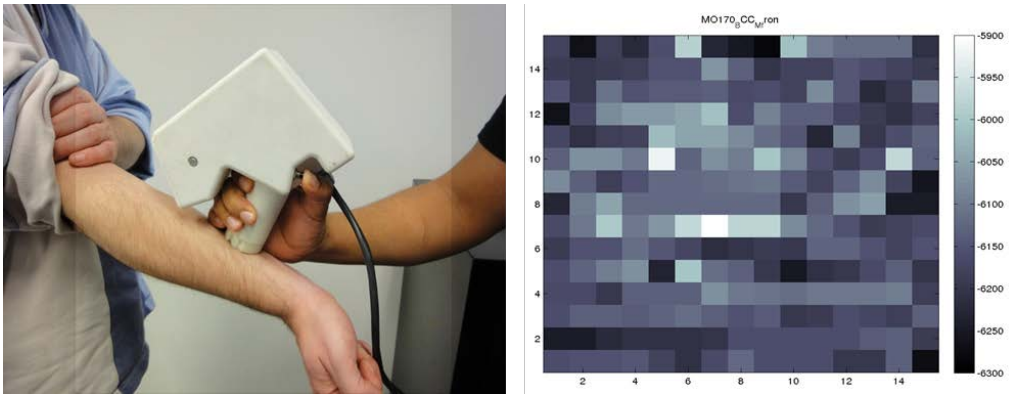

Figure 4. OFI system and 2D image of the lesion blood flow.

Since the three novel technologies included in the platform provided images, a scheme to enable correlation of the data collected from the different devices was finally designed. In this context, a metal ring was used enabling the acquisition of 3D, multispectral and OFI images. The ring was attached to the skin with a special double-coated adhesive to ensure that the location did not change during clinical measurements (Figure 5) and to know the orientation of the lesion.

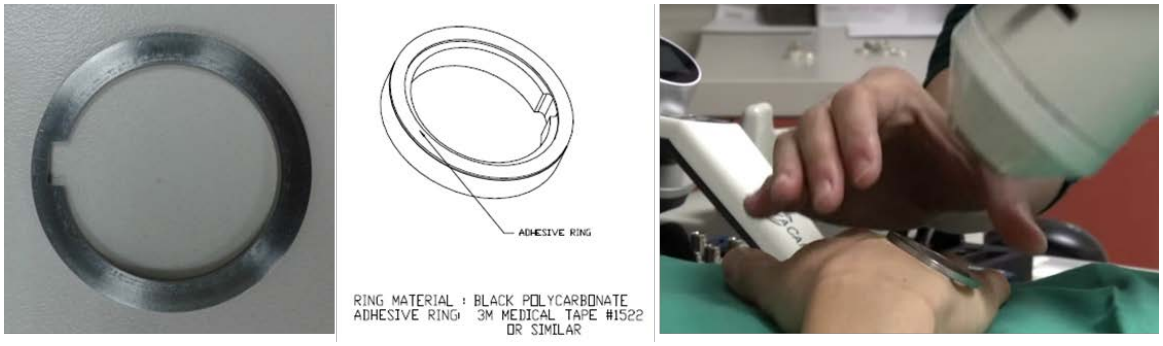


Figure 5. Metal ring used to correlate the information of the three novel systems.

Methods

From the 8 wavelengths (or spectral bands) available of the multispectral system, 8 reflectance and 8 absorbance images were computed. Then, three different groups of parameters were calculated from the reflectance images of a lesion. The first group consisted of the splined interpolation values (from 415 nm to 995 nm with steps of 10 nm) pixel by pixel of the 8 previous reflectance and absorbance images in order to obtain more accurate information. Additionally, differences between normal skin and the lesion were also computed in reflectance and absorbance terms to prevent the patient's skin from influencing the results.

The second group of parameters were computed to look for colour features of skin lesions; colour coordinates of standard colour representation spaces were used, such as those of the CIELAB colour space (CIE 142-2001), in which colour is represented with lightness (L*), red-green (a*), and yellow-blue coordinates (b*); alternatively, chroma ($C^*_{ab}$) and the hue angle can also be used ($h_{ab}$). More complex parameters based on colour differences (ΔE) between each pixel of the lesion and the averaged colour of the whole lesion were also

considered, as well as colour differences between each pixel of the lesion and the averaged colour of the surrounding healthy skin.

The third group consisted of what we considered *empirical parameters*, i. e., parameters empirically computed by operating with reflectance values at different wavelengths, the 8 initial wavelength of the system without interpolation, to enhance any particular spectral feature potentially different in healthy and malignant tissue that might be useful in discriminating among different types of skin lesions:

$$Par_m(i,j) = f\left(Refl_{\lambda n}(i,j)\right)$$

where $Par_m(i,j)$ is a particular parameter and $f\left(Refl_{\lambda n}(i,j)\right)$ is a function of the reflectance images computed from several wavelengths (they can be added, subtracted, multiplied etc.) in order to highlight subtle differences among lesions of different etiology. Various authors have suggested that some of these parameters can be useful to map a particular skin chromophore. For instance, Diebele et al, (Diebele et al. 2012) and Bekina et al, (Bekina et al. 2012) proposed parameters to account for bilirubin, erythema and a melanoma index.

Once all images including parameters from the three groups were obtained, a mask was created in order to segment the lesion from the skin. The segmentation algorithm consisted of maximizing the between-class variance of the lesion and the skin pixel values, from the intensity of the histogram at the bluest reflectance image (414 nm). Furthermore, for those lesions which had similar digital level than the skin or were not homogeneous, the reflectance image was divided into 4 different subimages, allowing to calculate different thresholds adapted to the different areas of the lesion.

Next, statistical descriptors were obtained for every segmented lesion for all parameters, i. e., mean ($\tilde{x}$), standard deviation (σ), maximum and minimum. As a first approach to the extraction of textural information, we used the analysis of the statistical properties of the histogram for any of the parameters calculated, also known as first order statistics (Gonzalez et al. 2004 and Ritter et al. 2001). This analysis includes the study of some features such as entropy (Ep), a well-known statistical measure of randomness, energy (En), a numerical descriptor of the image uniformity having 1 as its maximum value for a constant image, and the third central moment (μ3), which accounts for the skewness of the histogram. The mathematical description of these features are shown in the following equations:

$$Ep = -\sum_{i=0}^{n-1} P_i log_2(P_i)$$

$$En = \sum_{i=0}^{n-1} {P_i}^2$$

$$\mu_3 = -\sum_{i=0}^{n-1} (i-m)^3 P_i$$

where $n$ is the number of bins or intervals in which the histogram is divided into, $P_i$ is the relative frequency of the bin $i$ of the histogram and $m$ is the mean of the parameter.

Finally, a classification algorithm was developed to decide which lesions were malignant (melanomas and basal cell carcinomas) and which were benign (nevi). To this end, upper

and lower thresholds were firstly defined for each parameter as the interval limits that included all nevi. The upper (lower) threshold was chosen as the value of the nevus with the highest (lowest) value after some nevi were discarded according to the following formula:

$$Nevi\ outliers = \tilde{x}_{nevi} \pm 2 \cdot \sigma_{nevi}$$

where $\tilde{x}_{nevi}$ and $\sigma_{nevi}$ are the average and standard deviation, respectively, of each parameter calculated from all segmented nevi lesions. All lesions above or under the upper and lower thresholds for at least one parameter were classified as malignant.

Regarding the 3D system, from the 3D topography of each lesion measured, different processing algorithms were developed to extract parameters which characterize the morphology of the lesion. Using C++, Matlab and Mountains Map software programs, the lesion was segmented and 9 parameters were obtained: mean height, maximum height, width, perimeter, area, volume, and energy, entropy and 3$^{rd}$ central moment of the height distribution. The maximum and mean height, the width and the perimeter were calculated from the mean profile of a series of horizontal profiles of the lesion. The area and the volume were calculated using four different methods: vertical lines, horizontal lines, least squares planes and polynomial surface (of degree 2 and 6). Making the median of the five values, a single value of the area and volume were assigned to the lesion. The last three parameters were obtained from the histogram of the height distribution.

Taking the same idea as the classification algorithm to differentiate between malignant (melanomas and basal cell carcinomas) and benign (nevi) lesions in the multispectral system, thresholds were chosen according to the formula:

$$Nevi\ outliers = \tilde{x}_{nevi} \pm 2 \cdot M_{nevi}$$

where $\tilde{x}_{nevi}$ and $M_{nevi}$ are the average and mode, respectively, of each parameter calculated from all segmented nevi lesions. All lesions above or under the upper and lower thresholds for at least one parameter were classified as malignant.

Regarding the OFI system, from the signal obtained in the 255 points measured in each lesion, a 2D image of 15x15 pixels was obtained. However, due to the fact that the OFI system measured signal points and no image lesion was obtained, the position of the lesion highly uncertain. For this reason, a correlation between the OFI and the multispectral system was done, because the image position of the multispectral system and the area measured with the OFI inside the metal ring were known. However, due to mechanical behaviours, this correlation was not available until recently, and we are currently working on this. Figure 6 shows the Graphical User Interface (GUI) programmed with Matlab to correlate both systems information. The green square indicates the area measured with the OFI, and the broken green line is the area that has to be discarded due to its was not properly measured. The GUI allows to select the lesion, the centre of the lesion and the skin of the patient to create masks which will be multiplied by the 2D OFI image, previously adapted to the multispectral image dimensions. Next, statistical analysis with the information obtained will be done and also the classification algorithm will be applied, similarly to the multispectral and 3D systems.

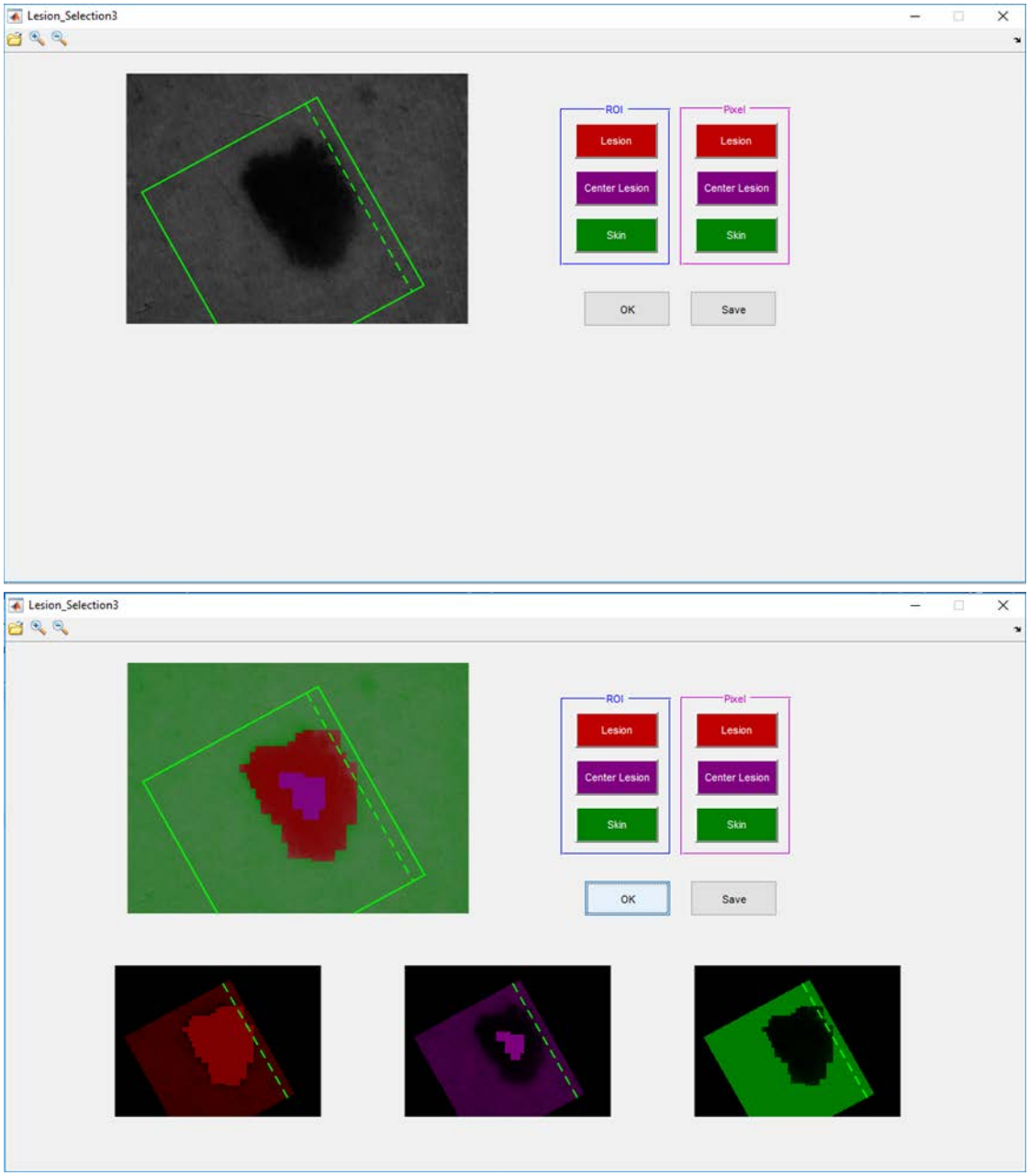


Figure 6. Graphical User Interface (GUI) to correlate the OFI information with the multispectral image.

**Description of the main results obtained:**

From all parameters calculated of the multispectral system, only 22 were finally selected to be used in the classification algorithm:

- Eleven from the first group (spectral reflectance and absorbance of the lesion; and corresponding differences between the lesion and the surrounding healthy skin): Ep of $Abs_{445}$, Ep of $Abs_{905}$, μ3 of $Refl_{665}$ and $\tilde{x}$ of $Refl_{555}$. Also, differences between lesion and surrounding skin in terms of Ep of $Abs_{425}$, En of $Abs_{465}$, μ3 of $Abs_{925}$ and μ3 of $Abs_{955}$, En of $Refl_{445}$, μ3 of $Refl_{525}$ and μ3 of $Refl_{935}$.

- Six were colour-based parameters (second group): maximum of a*, En of b*, En and minimum of C*; and σ of h* as CIELAB colorimetric coordinates, and maximum ΔE with the surrounding healthy skin as the reference.
- Five were empirical parameters (third group): maximum of Emp1, minimum of Emp2, minimum of Emp3, minimum of Emp4 and σ of Emp5, which are defined as follows:

$$Emp1 = Refl_{671}(i,j) \cdot (Refl_{995}(i,j)/Refl_{524}^2(i,j)) , \quad (11)$$

$$Emp2 = Refl_{524}(i,j)/(Refl_{671}(i,j) \cdot Refl_{995}(i,j)) , \quad (12)$$

$$Emp3 = Refl_{671}(i,j)/Refl_{524}(i,j) , \quad (13)$$

$$Emp4 = Refl_{671}(i,j)/Refl_{995}(i,j) , \quad (14)$$

$$Emp5 = Refl_{524}(i,j)/(Refl_{447}(i,j) \cdot Refl_{890}(i,j)) , \quad (15)$$

The following scatter plots (Figure 7) show 3 specific examples from the 3 groups of selected parameters and the corresponding upper and lower thresholds used for classification. The plots show that some of the melanomas and basal cell carcinomas tend to have higher values than nevi in the three cases.

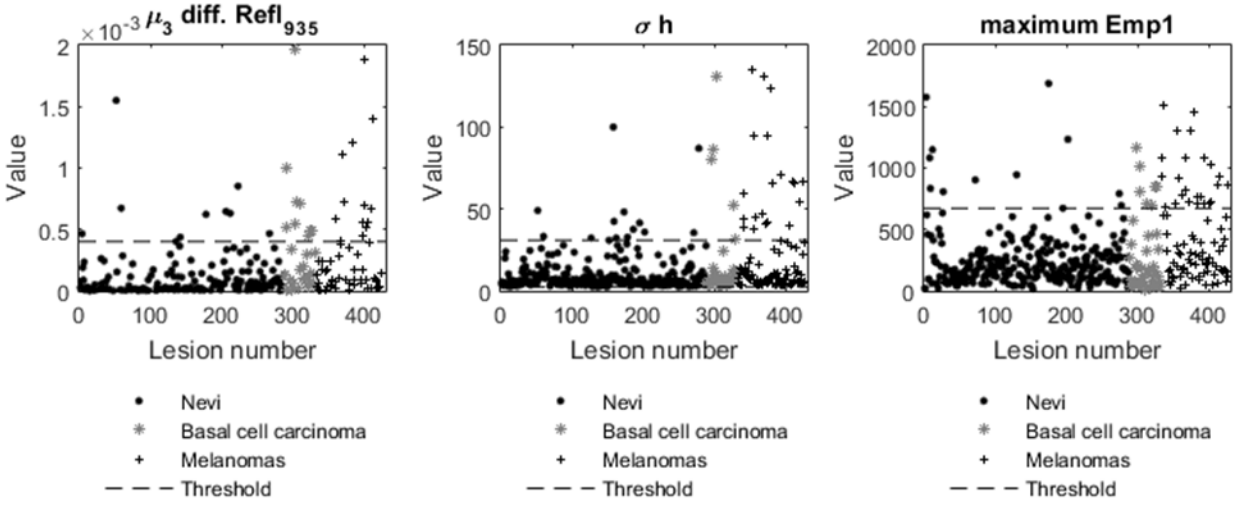


Figure 7. Scatter plots from 3 specific parameters: (a) differences between the lesion and the skin in terms of μ3 of Refl935 (b) σ of hue angle h of the CIELAB color space and (c) maximum of Emp1.

With the classification algorithm based on these 22 parameters, 8 out of 95 melanomas and none of the 44 basal carcinomas were misclassified (94.24% sensitivity); in contrast, 130 nevi from 290 were classified as malignant (55.17% specificity). Here, sensitivity or true positive rate is the probability of detecting malignant lesions (melanomas and basal cell carcinomas) and specificity or true negative rate is the proportion of nevi correctly identified.

Regarding the 9 parameters from the 3D system, only 3 were selected: energy and the mean of the height distribution, and the perimeter, obtaining thus, a sensitivity of 79.5% and specificity of 59%.

By applying the method of the threshold and combining the parameters computed by the multispectral and the 3D system, the sensitivity slightly increased to 95.2% and specificity improved to 56.8%.

Further work will focus in the analysis of the OFI system and its combination with the multispectral and 3D systems.

**References:**


Delpueyo, X., Vilaseca, M., Royo, S., Ares, M., Sanabria, F., Herrera, J., Pujol, J., Puig, S., Pellacani, G., Vázquez, J., Solomita G. and Bosch, T. (2016): *Sistema multiespectral para el diagnóstico del cáncer de piel*. XI Congreso Nacional del Color. 2016, Proceedings.

CIE 142-2001. Improvement to industrial colour-difference evaluation. ISBN: 9783900734602

Bekina, A., Diebele, I., Rubins, U., Zaharans, J., Derjabo, A., Spigulis, J., "Multispectral assessment of skin malformations using a modified video-microscope", *Latv. J. Phys. Tech. Sci.* **49**(5), 4-8, (2012).

Diebele I., Kuzmina I., Lihachev A., Kapostinsh J., Derjabo A., Valeine L, Spigulis J., "Clinical evaluation of melanomas and common nevy by spectral imaging" *Biomed. Opt. Express*, **3**(3), 467-472, (2012).

Bosch, T., Servagent, N. & Donati, S., 2001. Optical feedback interferometry for sensing application. *Optical Engineering*, 40(1), p.20.

Moreira, R.C. et al., 2016. An embedded 2D imager for microscale flowmetry based on Optical Feedback Interferometry. , pp.5–7.

Ares, M. et al., 2014. Handheld 3D Scanning System for In-Vivo Imaging of Skin Cancer. *Proceedings of the 5th International Conference on 3D Body Scanning Technologies, Lugano, Switzerland, 21-22 October 2014*, (October), pp.231–236. Available at: http://www.3dbodyscanning.org/cap/abstracts/2014/231ares.html.

Zhang, S., 2010. Recent progresses on real-time 3D shape measurement using digital fringe projection techniques. *Optics and Lasers in Engineering*, 48(2), pp.149–158. Available at: http://dx.doi.org/10.1016/j.optlaseng.2009.03.008.

Chen, L. et al., 2005. Fringe contrast-based 3D profilometry using fringe projection. *Optik*, 116(3), pp.123–128.

Laveau, S. & Faugeras, O.D., 1994. 3-D scene representation as a collection of images. *Proceedings of 12th International Conference on Pattern Recognition*, 1, pp.689–691.

**Mutual benefits for the Home and Host institutions:**

This visit resulted an exchange of knowledge regarding multispectral system, 3D imaging and optical feedback interferometry.

**Future collaboration with the Host institution (if applicable):**

In the near future further results will be obtained with the combination of the three novel technologies presented.

**Foreseen journal publications or conference presentations expected to result from the STSM (if applicable):**

Depending on the final results, conference proceedings or journal articles will be considered.

Part of these results (those concerning the multispectral system) have been recently submitted to the Journal of Biomedical Optics and are now under revision.

**Connect also this to the results.**

- ***Innovative knowledge resulting from COST networking through the Action. (Specific examples of Results vs. Objectives)***

The techniques developed from both partners of the COST network (Host and Home Institution) have been successfully combined. Multispectral and 3D systems have been entirely combined and results in terms of sensitivity and specificity have been provided in this report. The same analysis but with the OFI systems are currently being done (not finished yet).

- ***Significant scientific breakthroughs as part of the COST Action. (Specific examples)***

Many different partners of the COST Action have participated directly or indirectly in this mission. Home and host institutions as techniques' developers and the two hospitals as clinical partners. This has allowed applying novel photonic and optical techniques to the diagnosis of skin cancer, which was not tested before.

- ***Tangible medium term socio-economic impacts achieved or expected. (Specific examples)***

The results of this study can have a strong impact in the society as between 2 and 3 million of skin cancers occur globally each year. One in every three cancers diagnosed is a skin cancer. Melanomas and Basal Cell Carcinomas have been classified in this study with promising results in terms of sensitivity and specificity that can improve that obtained nowadays by means of dermatoscopy.

# *STSM outcome form*

| STSM application number | Home institution & country | Host institution & country | BM1205 WG |
|---|---|---|---|
| COST-STSM-BM1205-36070 | UPC-CD6, Barcelona, Spain | LAAS-CNRS, TOULOUSE, FRANCE | WG1 |

## Objective of the collaboration

Analysis of data acquired with a multiphotonic platform for in-vivo imaging of skin cancer lesions

## Results of the collaboration

By combining the parameters computed by a multispectral and a 3D imaging system, the sensitivity increased to 95.2% and specificity improved to 56.8%.

Further common work will focus in the data analysis of an Optical Feedback Interferometer and its combination with both systems to ameliorate the robustness of the diagnosis.

*I hereby confirm the successful execution of the STSM of Ms Xana Delpueyo from* 17th December to 17th March in LAAS-CNRS, University of Toulouse, France.

*Yours sincerely,*

*Signature:*

Prof. Thierry BOSCH,
Université de Toulouse, INPT
Head of the Research Group of Optoelectronics for Embedded Systems, LAAS-CNRS.
Director of the Joint Laboratory CapIRO (INPT-CNRS-ACOEM Group)